P1.24 **ASSESSMENT OF FORCING DATA DERIVED FROM ECMWF MODEL FOR SCMS AT THE ARM SGP SITE**

Shaocheng Xie*, Richard T. Cederwall, J. John Yio
Lawrence Livermore National Laboratory, Livermore, CA

Minghua Zhang
State University of New York, Stony Brook, NY

1. INTRODUCTION

The Single-Column Model (SCM) is a useful tool to test and evaluate physical parameterizations used in climate models (Randall et al., 1996). A successful SCM test requires highly accurate large-scale forcing data, such as the large-scale advective tendencies of temperature and moisture and vertical velocity. These forcing data can be derived from the data collected in major field programs (e.g., Atmospheric Radiation Measurement program, ARM; and Tropical Ocean-Global Atmosphere Coupled Ocean-Atmosphere Response Experiment, TOGA-COARE) through objective analysis. However, the observations are often available only over a limited time periods and regions. Over regions and periods where observations are not available or data density is low, large-scale forcing data must be derived from output of operational numerical weather prediction (NWP) models (e.g., Iacobellis et al., 2002). A potential problem in using the NWP data is that the forcing data themselves are affected by deficiencies of the model physical parameterizations used in generating the data. However, how much model physical parameterizations influence these forcing fields and how the forcing data affect SCMs results have not been discussed previously in the literature.

In this paper, we attempt to address the above issues through assessment of the forcing data diagnosed from the European Center for Medium Range Weather Forecast (ECMWF) model by using data collected from the ARM Intensive Operational Periods (IOPs) and processed by the ARM objective variational analysis (Zhang and Lin, 1997; Zhang et al., 2001). We will also present results from SCM tests to demonstrate impacts of using NWP forcing on SCM simulations.

* *Corresponding author address:* Shaocheng Xie, Lawrence Livermore National Laboratory, Atmospheeric Science Division, Livermore, CA 94550; e-mail: xie2@llnl.gov

2. LARGE-SCALE FORCING

2.1 Observed forcing

The observed forcing fields are derived from the data collected during the ARM summer 1997 IOP, from 17 June (2330 UTC) to 17 July (2330 UTC), and winter 2000 IOP, from 27 Nov. (1730 UTC) to 22 Dec. (0830 UTC) at Southern Great Plains (SGP) site, using the constrained variational analysis approach developed in Zhang and Lin (1997). The variational analysis approach uses the domain-averaged surface precipitation, latent and sensible heat fluxes, and radiative fluxes at the surface and Top of the Atmosphere (TOA) as the constraints, to enforce the atmospheric state variables to satisfy the conservation of mass, heat, moisture and momentum. Therefore, the derived dataset from this approach is dynamically and thermodynamically consistent. Many studies have shown that this approach significantly improves the accuracy of the large-scale forcing and its derived forcing datasets are widely used in the current SCM studies (e.g., Ghan et al., 2000; Xie et al., 2002). Fig. 1 displays the variational analysis domain that is circled by the analysis grids (+), which includes the five ARM sounding stations and seven wind profiler stations.

2.2 ECMWF forcing

ECMWF has been providing ARM with continuous datasets including the large-scale forcing data, covering all the three ARM field research sites: North Slope Alaska (NSA), SGP, and Tropical Western Pacific (TWP) since 1995. The model forcing is diagnosed from the ECMWF model runs that are specifically extracted to force SCMs. These data are averaged over an area that is close to the ARM variational analysis domain (see Fig. 1). The dataset is a composite of 12 to 36 hour forecasts. The model used to generate the dataset is the ECMWF global spectral model. Detailed information can be found in the release notice for the SGP ECMWF data sets at: www.arm.gov/docs/xds/static/ecmwf.html. Information about the model physical parameterizations can be seen in Gregory et al. (2000).

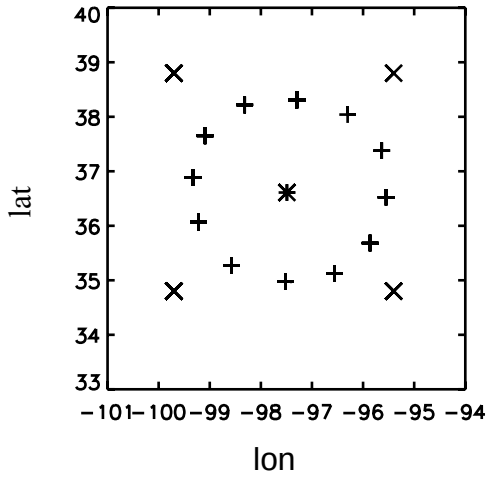

Fig. 1. The boundary locations of the ARM SCM variational analysis domain (+) and the ECMWF analysis domain (x). Central facility is represented by *.

3. RESULTS

In this study, a strong convective subperiod from 23 June (2330 UTC) to 29 Jun (2330 UTC) during the Summer 1997 IOP and a non-convective subperiod from 27 Nov. (1730 UTC) to 3 Dec. (1730 UTC) during the Winter 2000 IOP are selected to assess the ECMWF derived forcing under different weather conditions.

3.1 Convective case

The convective period contained two strong precipitation events on June 25 and 29 and a weak precipitation event on June 27 (Fig. 2, blue line). These convective events were associated with mesoscale convective systems that were influenced by the large-scale circulations. It is seen that the model largely underestimates the observed precipitation (red line in Fig. 2) and tends to trigger convection earlier than the observations. Note that strong convective events are generally associated with the large-scale dynamic processes such as large-scale upward motion and low-level moisture convergence. The failure to correctly reproduce the observed precipitation, which is related to deficiencies of the model parameterizations, has large impact on the diagnosed vertical velocity and advective tendencies as discussed later.

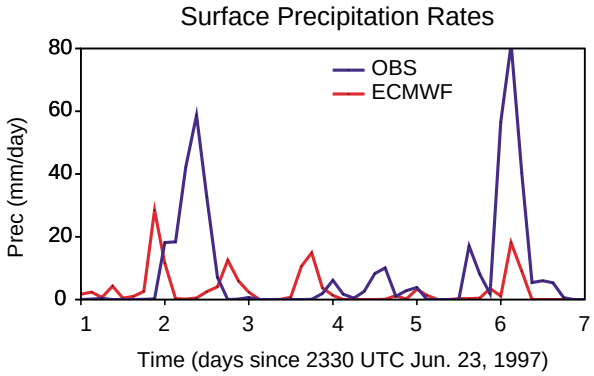

Fig. 2. Time series of the observed (blue) and ECMWF model produced (red) surface precipitation rates

To assess the ECMWF diagnosed forcings, we first examine the column-integrated heat and moisture budgets:

$$Cp\frac{\partial < T >}{\partial t} + Cp < \nabla \cdot \vec{V}T >= R_{TOA} - R_{SRF} + LP_{rec} + SH + L\frac{\partial < q_l >}{\partial t} \quad (1)$$

$$\frac{\partial < q >}{\partial t} + < \nabla \cdot \vec{V}q >= E_s - P_{rec} - \frac{\partial < q_l >}{\partial t} \quad (2)$$

where

$$< X >= \frac{1}{g}\int_{p_t}^{p_s} (X)dp$$

where $\vec{V}$ is the wind, T is the temperature, q is the mixing ratio of water vapor, p_s is the surface pressure and p_t is the TOA pressure, q_l is the cloud liquid water content, R is the net downward radiative flux at TOA and at the surface (SRF), P_{rec} is precipitation, L is the latent heat of vaporization, C_p is the heat capacity, SH is the sensible heat flux, and E_s is the surface evaporation. Note that the terms on the right-hand side of the equations are the constraints used in the variational analysis. These constraints are not changed in the analysis.

Table 1 lists the statistics of the observed (values in parenthesis) and model calculated column heat and moisture budget components during the convective period. The observed values are obtained from the variational analysis. In the table, 'mean' represents an a time average of the 3-hourly observed values and 1-hourly model calculated values over the convective period, 'std' represents standard deviation, 'rmse' is Root-Mean-Square (RMS) error, and 'coef' is the correlation coefficient. Since cloud liquid term is very

small compared to other terms, it is not shown in the table. The budget check shows that the column-integrated energy and moisture budgets are balanced in the constrained variational analysis. The area-averaged ECMWF model data also conserve well the column energy budget with period-mean budget imbalance about 1.45 W m^{-2}. For the column moisture budget, we are not able to check due to the lack of the model calculated evaporation. The E_s shown in Tables 1 and 2 are diagnosed from the column-integrated moisture budget by assuming the budget is in balance. This assumption should not introduce large errors in the diagnosed evaporation since the column moisture balance should be guaranteed in the original ECMWF model.

Table 1. Comparison of ECMWF model data to the ARM observations (values in parenthesis) for the column-integrated heat and moisture budget components during the convective period (w m^{-2})

	Mean	std	rmse	coef
R_{TOA}-R_{SRF}	-97.7 (-57.1)	127. 9 (162.1)	63.8	0.97
L*PREC	90.8 (261.8)	163.6 (517.4)	533.3	0.20
SH	27.8 (40.8)	76.9 (46.6)	42.4	0.90
E_s	145.2 (109.6)	148.8 (111.9)	62.2	0.96
$C_p^* \partial\langle T\rangle/\partial t$	13.7 (33.6)	284.1 (247.6)	165.9	0.81
$C_p^* \langle \nabla \cdot \vec{V}T \rangle$	8.8 (210.7)	254.5 (519.4)	608.7	0.23
$L^* \partial\langle q\rangle/\partial t$	11.8 (26.5)	271.1 (225.6)	329.7	0.11
$L^* \langle \nabla \cdot \vec{V}q \rangle$	42.6 (-178.6)	355.5 (519.4)	558.6	0.34

It is seen from the table that significant disagreements exist in both the constraint variables and the derived fields between the model and the observations. For those constraint variables, the model largely overestimates the column net radiation and surface evaporation while it significantly underestimates the latent and sensible heat fluxes in terms of the period-mean values. The largest error is in the calculated latent heat flux, which shows a bias of approximately 65% of the observed mean. The RMS error of this term is also very large and is similar to the magnitude of the temporal variability in the observations. Its correlation coefficient with the observations is quite small (0.2). It should be noted that these constraint variables used in the variational analysis are obtained directly from the observations and are not changed during the variational analysis. Therefore, the discrepancies in these variables between the model and variational analysis reflect deficiencies of the model parameterizations. As shown in Zhang et al (2001), these constraint variables can make large differences in the diagnosed large-scale vertical velocity and advective tendencies.

Consistent with above discussions, the model diagnosed forcing fields, i.e., the column-integrated horizontal heat and moisture convergences ($C_p^* \langle \nabla \cdot \vec{V}T \rangle$ and $L^* \langle \nabla \cdot \vec{V}q \rangle$), are largely different from those derived from the objective variational analysis. It is seen that the variational analysis shows very strong horizontal advective cooling and large moisture convergence during the strong convective period, which agree with many observations, while the model exhibits rather weak advective cooling and weak divergence, instead of convergence, in the moisture budget. Clearly, this is partially related to the problems in the model predicted surface precipitation as we showed in Fig.2. The magnitudes of the temporal variability in these two diagnosed fields are much weaker than those in the variational analysis data. The RMS errors are large, similar to the observed standard deviations, and the correlation coefficients are very small (0.23 and 0.34).

It is noted that the heat and moisture storage terms $C_p^* \partial\langle T\rangle/\partial t$ and $L^* \partial\langle q\rangle/\partial t$ show noticeably different between the model and the observations, even though the model time averaged temperature and moisture agree well with the observations with errors of less than 0.5 K in temperature and 0.3 g kg^{-1} in moisture, respectively.

Another noteworthy feature is that, for the variational analysis during the convective period, the latent heat flux and the horizontal advective cooling are the two largest terms to balance each other in the energy budget, and the surface precipitation and the horizontal moisture convergence are the two largest terms to balance each other in the moisture budget. For the model, however, the latent heat flux is balanced by the column net radiative cooling, and the surface precipitation and the horizontal moisture divergence are balanced by the surface evaporation. The relationships presented in the model calculated column-integrated budgets of heat and moisture during the strong convective events are often not supported by observations.

Although there are large disagreements between the model and the observations, it is interesting to see that the model calculated column net radiation, sensible heat flux, and evaporation terms show rather high correlation (above 0.9) with the observations. This is mainly because these processes are largely dominated by the strong solar diurnal variations over the midlatitude land in the summer.

The time-height distributions of the derived vertical velocity and the total advective tendencies of temperature and moisture from the variational analysis are shown in Figs. 3a-c for the convective period. Note that the total advection of temperature includes the adiabatic expansion/compression term. Corresponding to the observed surface precipitation events (Fig. 2), the derived forcings show strong large-scale advective cooling (associated with strong upward motion) in the

middle and upper troposphere and strong moisture convergence in the lower troposphere.

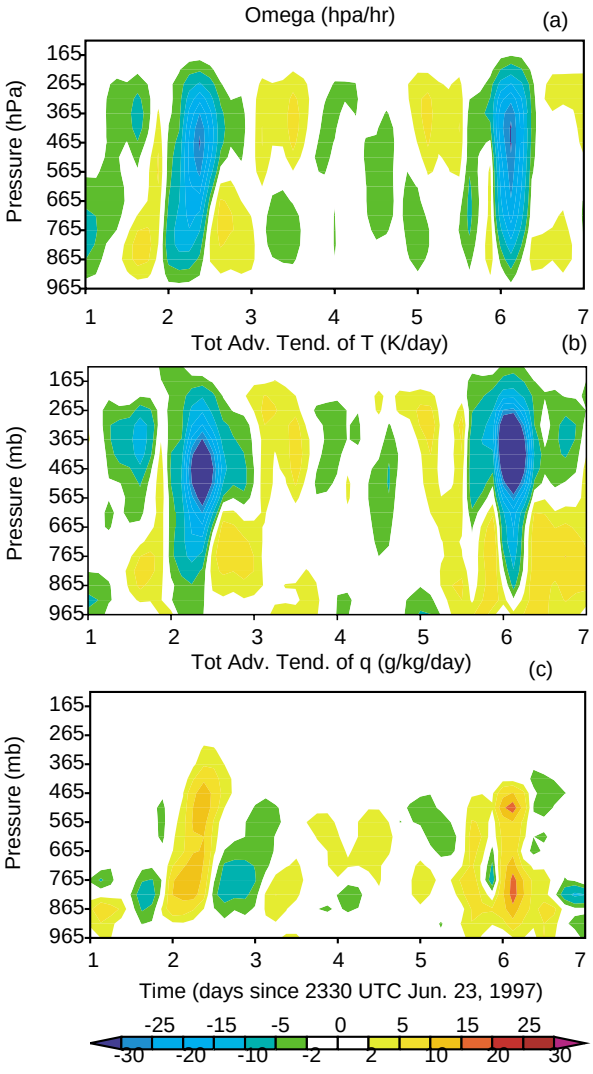

Fig. 3. The time-height distributions of the derived vertical velocity (a), total advective tendencies of temperature (b) and moisture (c).

Figs. 4a-c are the same as Figs. 3a-c except they are for the model derived forcing fields. In this case, the model derived forcing fields are closely associated with the calculated precipitation. As we showed earlier, however, the calculated precipitation events are much weaker than the observations and also are triggered too early. Associated with these problems, the model derived forcing fields are much weakercompared to those derived from the variational analysis. For some periods, such as on day 2, in which a strong convective event was observed, the two different forcings are even out of phase. On this day, the objectively analyzed data show very strong upward motion and advective cooling in the middle and upper troposphere and large lower-level moisture convergence while the ECMWF data displays weak

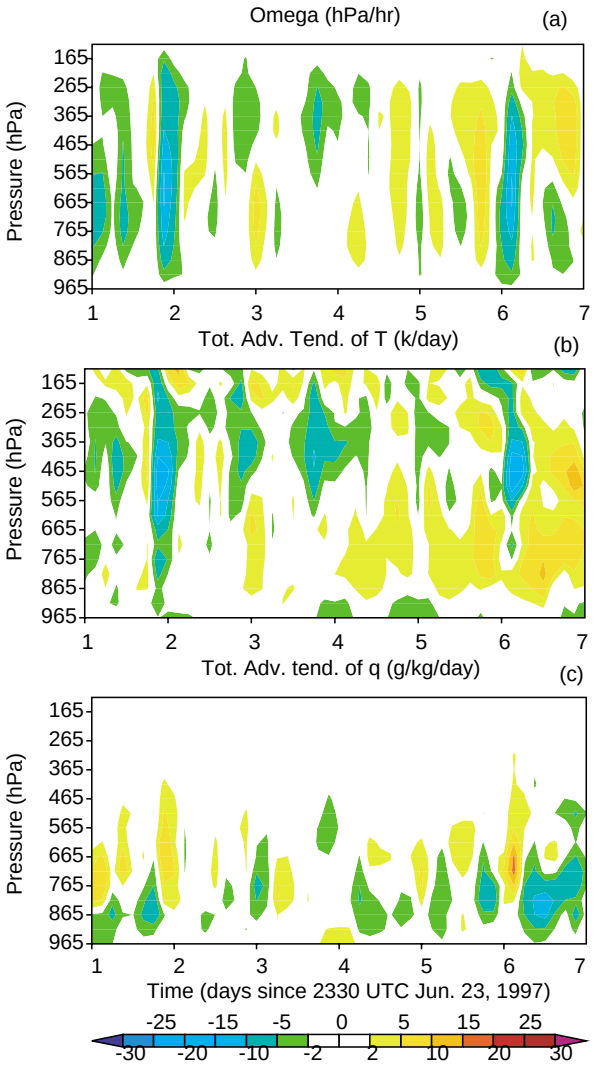

Fig. 4. Same as Fig. 3 except for ECWMF derived forcing fields.

downward motion and small advective heating in the middle and upper troposphere and weak lower-level moisture divergence. In this case, the variational analysis diagnosed forcing fields exhibit more realistic large-scale dynamical and thermodynamic structures for the convective system.

3.2 Non-convective case

The statistics of the model calculated column heat and moisture budget components during the non-convective subperiod of the winter 2000 IOP are listed in Table 2. The corresponding components from the variational analysis are shown in parenthesis. For the non-convective case, the disagreements of the model

calculated budget components from the observations are significantly smaller than those in Table 1. For the constraint variables, the calculated column net radiation agrees well with the observation, with error less than 7% of the observed value. The model-produced spurious precipitation is very small (0.83 w m^{-2} ~ 0.03 mm day^{-1}) and can be neglected. In contrast, relatively larger errors are seen in the sensible heat flux and surface evaporation, especially in the latter. The model typically shows good correlation with the observations for the constraint variables, especially for the column net radiation, for which its correlation coefficient is 0.96.

For the diagnosed heat and moisture convergences, the model derived fields show similar temporal variability as those in the variational analysis data. The RMS errors are smaller than the magnitudes of the observed temporal variability. The correlation coefficients are 0.94 and 0.88, respectively. Yet, discrepancies in the mean diagnosed heat and moisture convergences are still noticeably large.

Another noticeable feature in Table 2 is that, during the non-convective period, both the model and the variational analysis show that the increase in the heat storage is balanced by the horizontal advective heating and column radiative cooling, and the decrease in the moisture storage is balanced by the moisture divergence and surface evaporation.

Figures 5a,b respectively display the total large-scale advective tendencies of temperature derived from the variational analysis and the ECMWF model during the non-convective period. The model derived forcing agrees well overall with the variational analysis forcing except for the levels above 215 hpa where the forcing derived from the model is stronger and has higher variability. This is partly because TOA is set to 10 hpa in the model while it is set to 100 hpa in the variational analysis. Similar results can be seen in the total advection of moisture and vertical velocity fields (not shown).

Table 2. Same as Table 1 except for the non-convective period.

	mean	std	rmse	coef
R_{TOA}-R_{SRF}	-113.6 (-106.3)	65.4 (93.2)	35.8	0.96
L*PREC	0.83 (0)	2.9 (0)	3.1	N/A
SH	8.2 (12.5)	66.2 (68.8)	37.6	0.84
E_s	26.9 (14.8)	38.6 (18.3)	26.8	0.88
$C_p^* \partial\langle T\rangle/\partial t$	-32.6 (-37.9)	256.7 (294.5)	104.8	0.94
$C_p^* \langle \nabla \cdot \vec{V}T\rangle$	-71.6 (-55.9)	224.7 (295.4)	117.9	0.93
$L^* \partial\langle q\rangle/\partial t$	-24.9 (-16.7)	171.0 (131.2)	80.2	0.89
$L^* \langle \nabla \cdot \vec{V}q\rangle$	51.1 (31.7)	163.2 (126.5)	81.2	0.88

3.3 SCM simulations

The NCAR CCM3 SCM with a modified cumulus convection scheme (Xie and Zhang, 2000) is used to investigate impacts of the different large-scale forcings derived from the ARM objective variational analysis and the ECMWF model on SCM simulations. In the SCM runs, the large-scale total advective tendencies of temperature and moisture are specified from these derived forcing fields. The surface forcing is calculated by the model surface parameterizations

Figures 6a,b give the simulated temperature and moisture biases averaged over the convective period during the summer 1997 IOP, respectively. It is seen that the SCM forced by the two different forcing data produces quite different results. The cold biases in the upper and lower troposphere (Fig. 6a) and the dry biases (Fig. 6b) in the lower troposphere are significantly larger in the simulations when the SCM is driven by the ECWMF derived forcing.

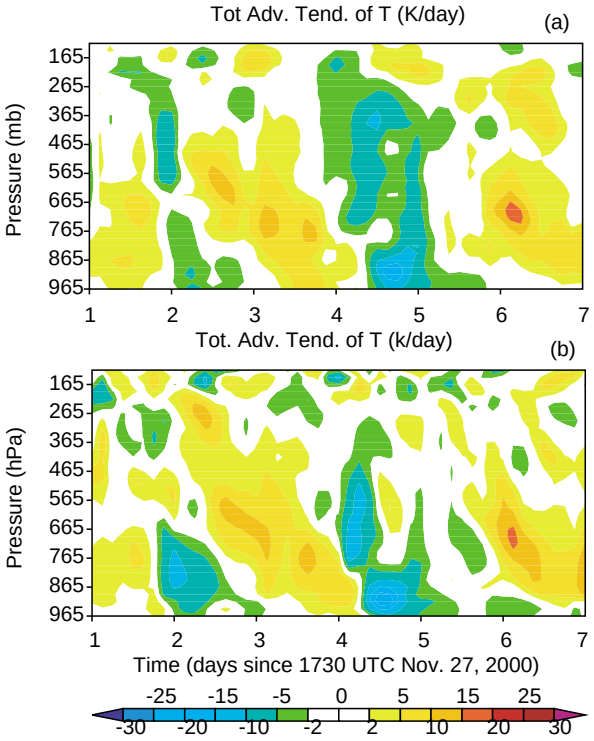

Fig. 5. The time-height distributions of the derived total advective tendencies of temperature. (a) Observations. (b) ECMWF.

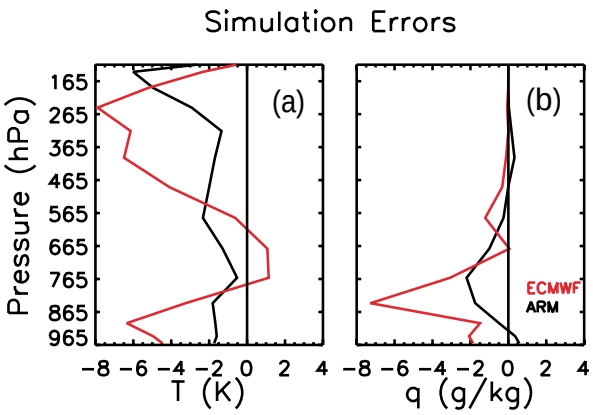

Fig. 6. The time-averaged temperature (a) and moisture (b) biases produced from the SCM forced by the ECMWF forcing (red) and the ARM variational analysis forcing (black) over the convective period.

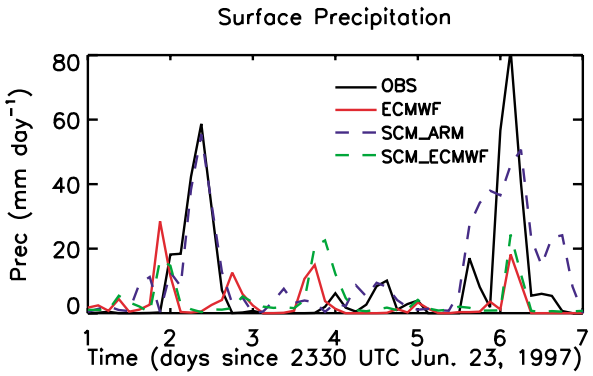

Fig. 7. The time series of the observed (black), ECMWF produced (red), and the SCM simulated surface precipitation (Cyan color for the ARM variational forcing and blue color for the ECMWF forcing.

The simulated surface precipitation rates by the SCM are shown in Fig. 7 for the convective case. The SCM driven by the variational analysis forcing generally reproduces well the observed precipitation. In contrast, the SCM with the ECMWF forcing largely underestimates the observed precipitation. Note that it reproduces well the ECMWF model predicted precipitation, which is expected. Similar results can be found in the simulated TOA longwave radiative fluxes (not shown).

The analysis presented above for the convective period highlights a problem when using the forcing derived from NWP models to run SCMs and then comparing the SCM results with observations. The NWP-derived forcing may not capture the effects of local convection that are present in the observations. Thus, when comparing SCM results with observations, it is difficult to partition the errors into that due to the forcing and that due to the parameterizations. It should be noted also that the errors could be compensating, which can make the SCM test results misleading. The most consistent use of NWP-derived forcing for the convective period is for comparisons of the SCM results with the NWP model results.

Figures 8a,b show the simulated temperature and moisture biases averaged over the non-convective period during the winter 2000 IOP. It is seen that the SCM with the ECMWF derived forcing shows large warm and moist biases below 550 hpa while the SCM with the variational analysis forcing produces large cold bias in the upper troposphere and warm bias between 650 – 850 hpa and very small moisture bias. Overall the SCM model simulation is comparable for the two different forcing data.

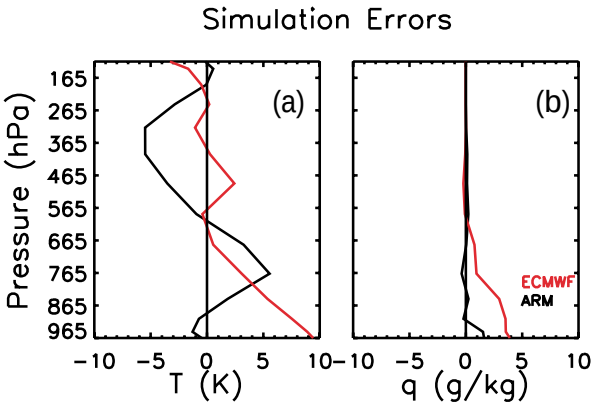

Fig. 8. The time-averaged temperature and moisture biases produced from the SCM forced by the ECMWF forcing (red) and the ARM variational analysis forcing (black) over the non-convective period.

4. DISCUSSION OF THE COMPARISON

It is noticed from Fig. 1 that the ECMWF domain is slightly larger than the variational domain. So one cannot expect the domain- averaged forcing fields derived from ECMWF are exactly the same as those from the variational analysis. However, the significant disagreements between these two types of forcing data shown during the convective period in this study cannot be easily explained by the differences in the size of averaging domains. Instead, they are clearly related to the imperfect model parameterizations that lead to the errors in those constraint variables in the column energy and moisture budgets, especially precipitation, which have large impact on the diagnosed large-scale forcing fields. An additional check for the ECMWF diagnosed forcing data averaged over a smaller domain shows very similar results.

Another concern for this comparison is that the objective analysis derived large-scale forcing fields may contain subgrid-scale information. This concern can be somewhat alleviated in this study because the variational analysis approach can automatically de-alias small-scale features from the instantaneous soundings by using the domain-averaged constraints

to diagnose the desired large-scale forcing fields. However, this approach cannot de-alias data in time and in the vertical direction. In the variational analysis, we have implemented vertical smoothing and time filtering techniques to reduce impacts of the small-scale noise on the derived large-scale forcing variables.

5. CONCLUSIONS

The large-scale forcing dataset diagnosed from the ECMWF model has been assessed under different weather conditions using data observed from a convective period during the ARM summer 1997 IOP and a non-convective period during the winter 2000 IOP at SGP. Over the convective period, we have shown that the ECMWF diagnosed forcing fields are much weaker than those derived from the ARM objective variational analysis. The correlation between these two different forcing data sets is quite small. These are closely related to the errors in the ECMWF model predicted surface precipitation. The errors in the model predicted surface latent and sensible heat fluxes, and surface and TOA radiative fluxes also influence the diagnosed forcing fields because these surface and TOA fluxes are the important components in the column-integrated budgets of heat and moisture. Over the non-convective period, the disagreements between these two forcing data sets are significantly smaller compared to those over the convective period. Also the two forcing data sets display high correlation, although differences between the ECWMF diagnosed data and the variational analysis data are still noticeable.

SCM tests have shown comparable simulation results when the SCM is driven by these different forcing data sets during the non-convective period. During the convective period, however, the SCM with forcing data diagnosed from ECMWF data exhibits larger simulation errors. It has been shown that the SCM with the ECMWF forcing tends to reproduce some important aspects of the ECMWF model simulated atmosphere (e.g., surface precipitation and radiative fluxes), which are different from the observations. During convective periods, forcing SCMs with NWP model-derived forcing is appropriate if the SCM results are to be compared with the NWP model results. However, if the SCM test involves comparison with observations, then use of NWP-derived forcing can lead to the SCM results that are inconclusive, whether the comparison appears good or bad. It is more suitable to use forcing derived from observations to run SCMs when comparing results with observations.

It should be noted that SCMs have stringent requirements for the large-scale forcing data. This study shows that the forcing data diagnosed from ECWMF data are generally reasonable over non-convective periods. Over strong convective periods, however, the model diagnosed forcing data show rather large disagreements with the variational analysis forcing and therefore the use of the model derived forcing data needs to be cautious. The ECMWF model nevertheless provides unique long-term continuous data set, including comprehensive information about the dynamical and physical fields, and there is no doubt that they are very useful for evaluation and development of parameterizations in climate models and understand the structure of large-scale systems and budgets.

ACKNOWLEDGEMENTS

This research was supported under the auspices of the U. S. Department of Energy by the University of California, Lawrence Livermore National Laboratory under contract No. W-7405-Eng-48. Work at SUNY Stony Brook was supported by ARM grant DE-FG02-98ER62570 and was also supported by NSF under grant ATM9701950. The ECMWF forcing data are obtained from the ARM data archive and provided by Dr. Christian Jakob, formerly of ECWMF and now Australian Bureau of Meteorology Research Centre.

REFERENCES

Ghan, S. J., et al., 2000: An intercomparison of single column model simulations of summertime midlatitude continental convection. *J. Geophys. Res.,* **105**, 2091-2124.

Gregory, D., J.-J. Morcrette, C. Jakob, A. M. Beljaars, and T. Stockdale, 2000: Revision of convection, radiation and cloud schemes in the ECMWF Integrated Forecasting System. *Q. J. R. Meteorol. Soc*., **126**, 1686-1710

Iacobellis, S. F., R. C. J. Somerville, 2002: Sensitivity of Radiation Fluxes and Heating Rates to Cloud Microphysics. *The Twelfth ARM Science Team Meeting Proceedings, St. Petersburg, Florida.*

Randall, D. A., K-M. Xu, R. J. C. Somerville and S. Iacobellis, 1996: Single-column models and cloud ensemble models as links between observations and climate models*. J. Climate,* **9**, 1683-1697

Xie, S. C., and M. H. Zhang, 2000: Impact of the convective triggering function on single-column model simulations. *J. Geophys. Res.,* **105**, 14983-14996

Xie, S. C., et al., 2002: Intercomparison and evaluation of cumulus parameterizations under summertime midlatitude continental conditions. *Q. J. R. Meteorol. Soc*., **128**, 1095-1135.

Zhang, M. H., and J. L. Lin, 1997: Constrained variational analysis of sounding data bases on column-integrated budgets of mass, heat, moisture, and momentum: Approach and application to ARM measurements. *J. Atmos. Sci.,* **54**, 1503-1524

Zhang, M. H., J. L. Lin, R. T. Cederwall, J. J. Yio, and S. C. Xie, 2001: Objective analysis of ARM IOP Data: Method and sensitivity. *Mon. Weather Rev., **129**,* 295-311.